

Acoustic beam steering by light refraction: Illustration with directivity patterns of a tilted volume photoacoustic source

Samuel Raetz, Thomas Dehoux, Mathieu Perton, Bertrand Audoin

▶ **To cite this version:**

Samuel Raetz, Thomas Dehoux, Mathieu Perton, Bertrand Audoin. Acoustic beam steering by light refraction: Illustration with directivity patterns of a tilted volume photoacoustic source. Journal of the Acoustical Society of America, 2013, 134 (6), pp.4381 - 4392. 10.1121/1.4828825 . hal-01889418

HAL Id: hal-01889418

https://univ-lemans.hal.science/hal-01889418

Submitted on 9 Oct 2018

HAL is a multi-disciplinary open access archive for the deposit and dissemination of scientific research documents, whether they are published or not. The documents may come from teaching and research institutions in France or abroad, or from public or private research centers.

L'archive ouverte pluridisciplinaire **HAL**, est destinée au dépôt et à la diffusion de documents scientifiques de niveau recherche, publiés ou non, émanant des établissements d'enseignement et de recherche français ou étrangers, des laboratoires publics ou privés.

Acoustic beam steering by light refraction: Illustration with directivity patterns of a tilted volume photoacoustic source

Samuel Raetz, Thomas Dehoux, Mathieu Perton,[a] and Bertrand Audoin[b]
Université de Bordeaux, Unité Mixte de Recherche, Centre National de la Recherche Scientifique 5295, I2M, 351 cours de la Libération, F-33400, Talence, France

(Received 16 May 2013; revised 9 September 2013; accepted 15 October 2013)

The symmetry of a thermoelastic source resulting from laser absorption can be broken when the direction of light propagation in an elastic half-space is inclined relatively to the surface. This leads to an asymmetry of the directivity patterns of both compressional and shear acoustic waves. In contrast to classical surface acoustic sources, the tunable volume source allows one to take advantage of the mode conversion at the surface to control the directivity of specific modes. Physical interpretations of the evolution of the directivity patterns with the increasing light angle of incidence and of the relations between the preferential directions of compressional- and shear-wave emission are proposed. In order to compare calculated directivity patterns with measurements of normal displacement amplitudes performed on plates, a procedure is proposed to transform the directivity patterns into pseudo-directivity patterns representative of the experimental conditions. The comparison of the theoretical with measured pseudo-directivity patterns demonstrates the ability to enhance bulk-wave amplitudes and to steer specific bulk acoustic modes by adequately tuning light refraction. © *2013 Acoustical Society of America*.
[http://dx.doi.org/10.1121/1.4828825]

PACS number(s): 43.38.Zp, 43.20.Rz, 43.35.Cg, 43.35.Ud [ANN] Pages: 4381–4392

I. INTRODUCTION

Controlling the directivity of electromagnetic and acoustic sources allows optimizing the design of resonant antennas,[1] spectral light multiplexing,[2] or developing accurate echolocation systems.[3] The manipulation of directivity also has crucial impacts on noise control applications[4] and oceanic and seismologic imaging.[5,6] For this, it is of utmost importance to understand and control the directivity. To this end, one can use phased array transducers,[7–12] move the source across the surface of the sample at a controlled speed,[13,14] compute virtual wavefronts in selected directions from measured acoustic surface displacements,[15] or design periodic surfaces[2] or metasurfaces[16,17] to create a network of surface sources. Also, in the case of laser-generated ultrasound, the interference of multiple pulsed laser beams can create a photoelastic phased array transducer to shape ultrasonic beams,[18] generate surface waves,[19] or transverse waves.[20]

All of these developments rely on the manipulation of surface sources. Here we present an alternative technique to steer the directivity of acoustic sources using a laser-generated sub-surface volume source. This approach takes advantage of the mode conversion at the surface to control the directivity of specific modes. To predict the directivity of such a volume source, we develop an analytical calculation.

To calculate directivity patterns in half-spaces, two main analytical approaches have been considered for several years. With asymptotic calculation of a complex-valued integral,[21] Miller and Pursey have studied several surface acoustic sources on a semi-infinite isotropic solid medium.[22] Thereafter, Lord developed an alternative calculation method based on the formalism of Green's functions and on a local formulation of the reciprocity theorem.[23,24] The formulation of the reciprocity theorem used by Lord[23] offers much simpler calculations of directivity functions compared to the integral method. In configurations with more sophisticated geometries or boundary conditions, such as in the case of a coated half-cylinder,[25] finite elements are commonly used to compute directivity patterns.

Such calculations have been used to predict the behavior of a variety of acoustic sources.[26–30] The directivity calculated for harmonic sources has notably been proved to be well suited to the description of pulsed acoustic sources, such as laser-generated thermoelastic sources.[31] On this ground, it has been demonstrated that surface thermoelastic sources could be modeled by a shear stress vector dipole.[32] It has also been shown that the directivity patterns obtained for a linear surface source or for a point surface source were identical.[32] The effects of thermal diffusion and of the lateral dimension of the source have been added in the calculations of directivity functions based on the method proposed by Miller and Pursey as well.[33] However, these works concern exclusively surface sources, and only few studies have included the effects of the optical penetration.[34]

To provide a deeper analysis of the effects of a distribution of acoustic sources within the bulk of the material and to investigate the ability of this distribution to control the generation of acoustic waves, a calculation method is developed to represent more complex in-depth source profiles. To this end, we present an approach based on the reciprocity

[a]Current address: Instituto de Ingeniería de la UNAM, Universidad Nacional Autónoma de México, Cd. Universitaria, Coyoacán 04510, México D.F., Mexico.
[b]Author to whom correspondence should be addressed. Electronic mail: bertrand.audoin@u-bordeaux1.fr

Redistribution subject to ASA license or copyright; see http://acousticalsociety.org/content/terms. Download to IP: 134.157.146.58 On: Fri, 10 Jan 2014 11:32:51

theorem and the superposition principle. For illustration, a laser beam obliquely incident on the surface of a semi-transparent material is used as a tilted thermoelastic volume source.

After the description of the geometry and of the hypothesis in Sec. II, we detail the calculation of the directivity patterns of a sub-surface volume source resulting from the absorption of an obliquely incident laser beam in Sec. III. In contrast to the standard analysis of directivity patterns for surface sources, we identify the new contributions to the directivity originating from mode conversion at the free surface in Sec. IV. This approach is first used to analyze the directivity patterns for symmetrical volume source (Sec. V), and it is then applied to analyze the effects of an asymmetrical acoustic source (Sec. VI). Finally the directivity patterns obtained by the present method are compared to experimental results obtained in a similar configuration[35] in Sec. VII. To do so, a transformation of the directivity patterns is required, notably to model the measurement of the displacement at a free surface of a plate.

II. DESCRIPTION OF THE OBLIQUE THERMOELASTIC SOURCE

In the literature on directivity patterns, the acoustic source is classically localized at the surface of the half-space.[22,23,31,32,36] Alternatively, we consider the acoustic generation through the expansion of a volume source here. The laser beam penetrates inside the material over a non-negligible optical skin depth. A volume of the material is heated and expands, which leads to the generation of acoustic waves. The acoustic source is thus distributed within the volume of the solid medium. Moreover, we include the angle of incidence of the laser beam. Note that in the remainder of this paper, all directivity functions are expressed in terms of the amplitude of displacements and not in intensity. The term "in amplitude" will be omitted in the following.

The problem geometry is schematized in Fig. 1. An isotropic half-space in $x_1 \geq 0$ is considered, with an incoming normal given by the unit vector $\mathbf{x}_1$. In the following, vectors are indicated by boldface. The origin O of the coordinate is placed on the surface of the halfspace. The unit vectors $\mathbf{x}_2$ and $\mathbf{x}_3$ complete the Cartesian system of reference coordinates (O, $\mathbf{x}_1$, $\mathbf{x}_2$, $\mathbf{x}_3$). The case of a laser beam focused to a line along the $\mathbf{x}_3$ direction is considered in order to simplify the geometry. Indeed as mentioned in the Introduction, under the assumption of an infinitesimal lateral extension, it has been demonstrated that the directivity patterns obtained for a linear surface source and for a point surface source are exactly the same, although the waveforms differ.[32] The geometry can then be considered as two-dimensional in a plane normal to the $\mathbf{x}_3$ direction, the longest dimension of the source. We have demonstrated in a previous paper[35] that the volume thermoelastic source is distributed along the direction of refraction of the laser beam, which forms an angle φ_r with $\mathbf{x}_1$. We also introduce the polar system of coordinates (O, $\mathbf{e}_r$, $\mathbf{e}_\theta$) for ease of calculation: the acoustic field is calculated at the point of observation M (R, θ) (Fig. 1), where R is constant and large enough for point M to be in the far field of the acoustic source.

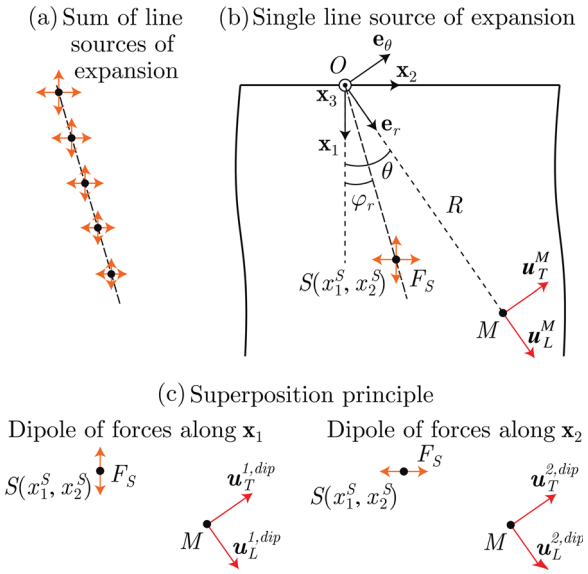


FIG. 1. (Color online) Decomposition of the problem for the calculation of directivity patterns of a tilted buried source layer: from the tilted buried source layer resulting of (a) a sum of line sources of expansion and (b) a single line source of expansion is considered to calculate the directivity pattern. (c) The superposition principle is used again to further simplify the calculation.

The amplitude of the acoustic source is directly proportional to the laser power density,[37] which decreases exponentially with depth. Its in-depth distribution is obtained by solving Maxwell's equation: $\beta(\varphi_r)\exp[-\beta(\varphi_r)x_1]$. The quantity $1/\beta(\varphi_r)$ corresponds to the projection along $\mathbf{x}_1$ of the optical penetration distance of the laser beam along the direction of refraction.[35] To simplify the analysis of directivity patterns, the lateral dimension of the source is neglected in this paper. The spatial distribution $s(x_1, x_2)$ of the acoustic source is therefore

$$s(x_1, x_2) = \beta(\varphi_r)\exp[-\beta(\varphi_r)x_1]\delta(x_2 - x_1 \tan\varphi_r), \qquad (1)$$

where the delta function δ describes the localization of the source along the direction of refraction.

III. CALCULATION OF DIRECTIVITY FUNCTIONS

To calculate the directivity functions, according to the superposition principle, we decompose the acoustic source into a sum of line sources of expansion parallel to the interface, buried and localized along the direction of refraction. This is schematized in Fig. 1(a). In contrast to the elementary buried line source, we refer to the complete thermoelastic source as the "buried source layer." The directivity of the tilted buried source layer is thus obtained from an integration of the directivities of each buried line source of expansion located at a varying distance from the surface.

A. Detailed methodology of calculation

Consider first the calculation of the radiation from a single buried line source of expansion of unit amplitude intersecting plane (O, $\mathbf{x}_1$, $\mathbf{x}_2$) at the point $S(x_1^S, x_2^S)$ [Fig. 1(b)].

Redistribution subject to ASA license or copyright; see http://acousticalsociety.org/content/terms. Download to IP: 134.157.146.58 On: Fri, 10 Jan 2014 11:32:51

The infinite line source is oriented along $\mathbf{x}_3$. We thus describe it as the sum of two dipoles oriented along $\mathbf{x}_1$ and $\mathbf{x}_2$ directions,[38] as schematized in Fig. 1(c). Since the solid medium is isotropic and the geometry is two-dimensional, only compressional (L) and in-plane shear (T) waves can be generated by the buried line source of expansion. Consequently, the calculation of four directivity functions $f_p^{q,\mathrm{dip}}$ is required, two for each dipole of forces in direction $q=\{1,\ 2\}$ corresponding to the two wave polarizations $p=\{L,\ T\}$. To obtain $f_p^{q,\mathrm{dip}}$, we calculate the displacement field $\mathbf{u}^{q,\mathrm{dip}}$ caused by a dipole of forces oriented along $\mathbf{x}_q$ and applied at the point S. Since $\mathbf{u}^{q,\mathrm{dip}}(M)$ is related to the displacement field $\mathbf{u}^{q,\mathrm{mono}}(M)$, caused by a single force of same amplitude, orientation, and applied at the same point S, by

$$\mathbf{u}^{q,\mathrm{dip}}(M)=\frac{\partial}{\partial x_q}\mathbf{u}^{q,\mathrm{mono}}(M), \tag{2}$$

it is sufficient to calculate $\mathbf{u}^{q,\mathrm{mono}}(M)$ at the point of observation M. The expression $f_p^{q,\mathrm{dip}}$ is eventually obtained by retaining the part of the amplitude of $\mathbf{u}^{q,\mathrm{dip}}(M)$ that depends on the angle of observation, thus rejecting the part of the amplitude that depends on the constant observation distance.

To summarize the methodology, the directivity functions of a buried line source of expansion are calculated by applying the following steps for each polarization $p=\{L,T\}$:

(i) Calculation of the displacement field $\mathbf{u}^{q,\mathrm{mono}}$ at the point of observation M caused by a *single force* of unit amplitude applied at point S in the direction $\mathbf{x}_q$.
(ii) Calculation of the directivity function $f_p^{q,\mathrm{dip}}$ of a *dipole of forces* of unit amplitude applied at point S in the direction $\mathbf{x}_q$ from Eq. (2) [Fig. 1(c)].
(iii) Application of the *superposition principle* to obtain the directivity function f_p^S of a line source of expansion located at point S [Fig. 1(b)],

$$f_p^S=f_p^{1,\mathrm{dip}}+f_p^{2,\mathrm{dip}}. \tag{3}$$

(iv) The directivity functions f_p^{OP} ($p=\{L,T\}$) of a tilted buried source layer are obtained by *integration* [Fig. 1(a)] of the directivity functions f_p^S of a single buried line source of expansion over the optical skin depth. f_p^S are multiplied by the spatial distribution s of the acoustic source [Eq. (1)],

$$f_p^{\mathrm{OP}}(\theta)=\int_{\mathbb{R}^+}\int_{\mathbb{R}} s(x_1^S,x_2^S)f_p^S(\theta,x_1^S,x_2^S)\,dx_2^S dx_1^S. \tag{4}$$

The particular form of the spatial distribution in our case, Eq. (1), leads to simplifications in Eq. (4),

$$f_p^{\mathrm{OP}}(\theta)=\int_{\mathbb{R}^+}\exp[-\beta(\varphi_r)x_1^S]f_p^S(\theta,x_1^S,x_2^S\tan\varphi_r)dx_1^S. \tag{5}$$

The building blocks of these equations are the displacement fields $\mathbf{u}^{q,\mathrm{mono}}$ caused by a single buried force of unit amplitude applied in the direction $\mathbf{x}_q$. Their calculation is now detailed.

B. Displacement field caused by a single buried force

The calculation of $\mathbf{u}^{q,\mathrm{mono}}(M)$ consists in calculating the displacement generated by a single force $\mathbf{F}^S$ along $\mathbf{x}_q$ applied at the point S of the half-space. The reciprocity theorem is very efficient to perform this calculation (see Sec. 5.8 in Ref. 36, for instance). It connects this initial problem to a reciprocal problem by a simple scalar equality detailed in the following. Choosing a reciprocal problem that is simple in its resolution then allows one to obtain results for the initial problem without complex calculations. We now express the reciprocal problem adapted to the initial problem of interest here.

Consider two harmonic forces $\mathbf{F}^S$ and $\mathbf{F}^M$, applied at the points S and M, respectively, of an elastic medium. The forces $\mathbf{F}^S$ and $\mathbf{F}^M$ cause displacements $\mathbf{u}(M)$ at point M and $\mathbf{u}(S)$ at point S, respectively. The reciprocity theorem can be summarized by the scalar relation

$$\mathbf{F}^S\cdot\mathbf{u}(S)=\mathbf{F}^M\cdot\mathbf{u}(M). \tag{6}$$

This is analogous to considering the equality between the virtual work developed by $\mathbf{F}^S$ over the displacement $\mathbf{u}(S)$ and the virtual work developed by $\mathbf{F}^M$ over the displacement $\mathbf{u}(M)$.[24] Equation (6) is now used to choose a reciprocal problem simpler to solve than the initial problem.

The initial problem to solve, in order to calculate the directivity for the compressional waves generated by a buried single force $\mathbf{F}^S$ applied at point S along $\mathbf{x}_1$, is to find the amplitude $u_L^{1,\mathrm{mono}}$ of the displacement at the point M along $\mathbf{e}_r$,

$$u_L^{1,\mathrm{mono}}=\mathbf{u}^{1,\mathrm{mono}}(M)\cdot\mathbf{e}_r. \tag{7}$$

The reciprocal problem we have chosen consists in a force $\mathbf{F}^M$ that generates a displacement $\mathbf{u}(S)$ at point S. According to the reciprocity theorem [Eq. (6)], choosing $\mathbf{F}^M$ such that $\mathbf{F}^M=\|\mathbf{F}^S\|\mathbf{e}^r$ yields the amplitude of $\mathbf{u}(S)$ in the direction of $\mathbf{F}^S$,

$$u_L^{1,\mathrm{mono}}=\mathbf{u}(S)\cdot\frac{\mathbf{F}^S}{F^S}=\mathbf{u}(S)\cdot\mathbf{x}_1. \tag{8}$$

Similarly, when the force $\mathbf{F}^S$ applied at the point S of the half-space is oriented along $\mathbf{x}_2$, application of the reciprocity theorem leads to the amplitude $u_L^{2,\mathrm{mono}}$ of the displacement at point M, along $\mathbf{e}_r$, generated by $\mathbf{F}^S$,

$$u_L^{2,\mathrm{mono}}=\mathbf{u}(S)\cdot\frac{\mathbf{F}^S}{F^S}=\mathbf{u}(S)\cdot\mathbf{x}_2. \tag{9}$$

Equations (8) and (9) show that the application of the reciprocity theorem allows one to switch the positions of the acoustic source and the position of the point of observation to form the simpler reciprocal problem. Since the point of observation in the initial problem is assumed to be in the far field of the source, the acoustic source in the reciprocal problem is far from the surface of the half-space. Therefore the acoustic waves reaching the surface, generated by the force at point M in the reciprocal problem, are acoustic plane waves. Thus, the reciprocal problem comes down to merely consider plane wave reflections at a free surface.

Redistribution subject to ASA license or copyright; see http://acousticalsociety.org/content/terms. Download to IP: 134.157.146.58 On: Fri, 10 Jan 2014 11:32:51

In the case of the force $\mathbf{F}^M$ of the reciprocal problem (a force of unit amplitude oriented along $\mathbf{e}_r$ and applied at point M), the displacement vector $\mathbf{u}$ (S) at point S caused by $\mathbf{F}^M$ is given by

$$\mathbf{u}(S) = U_{L_i} \sum_{L_i,L_r,T_r} R_m^{\parallel} e^{-\jmath k_1^m x_1^S} \mathbf{n}_m e^{\jmath(\omega t - k_2 x_2^S)}, \tag{10}$$

where index $m = \{L_i, L_r, T_r\}$ is associated either to the incident plane compressional wave (L_i), the reflected plane compressional wave (L_r), and the reflected plane shear wave (T_r) resulting from mode conversion at the free surface, respectively. In Eq. (10), U_{L_i} is the amplitude of the incident plane compressional wave and does not depend on θ. Therefore the expression of U_{L_i} is not important for directivity considerations. The quantities k_1^m and k_2 are the projections of the three wave vectors $\mathbf{k}_m$ along $\mathbf{x}_1$ and $\mathbf{x}_2$, respectively. Vectors $\mathbf{n}_m$ are the polarization vectors. The acoustic pulsation is denoted ω. Factors $R_m^{\parallel}$ represent the reflection coefficients of the plane waves reflected at a free surface.[38] Thus, Eq. (10) introduced in Eq. (8), respectively, Eq. (9), allows one to obtain the amplitude $u_L^{1,\text{mono}}$, respectively, $u_L^{2,\text{mono}}$, of the displacement along $\mathbf{e}_r$ at the point M caused by a single force of unit amplitude oriented along $\mathbf{x}_1$, respectively, $\mathbf{x}_2$.

C. Directivity function of a buried dipole of forces

The derivatives of $u_L^{1,\text{mono}}$ with respect to x_1 and of $u_L^{2,\text{mono}}$ with respect to x_2 lead to the analytical expressions of the two directivity functions for compressional waves, i.e., $f_L^{1,\text{dip}}$ and $f_L^{2,\text{dip}}$, associated with the dipoles of forces at the point $S(x_1^S, x_2^S \tan\varphi_r)$ along $\mathbf{x}_1$ and $\mathbf{x}_2$, respectively,

$$f_L^{1,\text{dip}} = \sum_{L_i,L_r,T_r} \jmath k_1^m n_1^m R_m^{\parallel} e^{-\jmath(k_1^m + k_2 \tan\varphi_r) x_1^S}, \tag{11a}$$

$$f_L^{2,\text{dip}} = \sum_{L_i,L_r,T_r} \jmath k_2 n_2^m R_m^{\parallel} e^{-\jmath(k_1^m + k_2 \tan\varphi_r) x_1^S}. \tag{11b}$$

The two directivity functions for shear waves $f_T^{1,\text{dip}}$ and $f_T^{2,\text{dip}}$ associated with the dipoles of forces in the initial problem applied at point S along $\mathbf{x}_1$ and $\mathbf{x}_2$, respectively, are obtained similarly. However, the single force applied at point M in the reciprocal problem is oriented along $\mathbf{e}_\theta$ instead of $\mathbf{e}_r$, and the plane acoustic wave incident on the free surface is now a shear wave. The analytical expressions for $f_T^{1,\text{dip}}$ and $f_T^{2,\text{dip}}$ are

$$f_T^{1,\text{dip}} = \sum_{T_i,L_r,T_r} \jmath k_1^m n_1^m R_m^{\perp} e^{-\jmath(k_1^m + k_2 \tan\varphi_r) x_1^S}, \tag{12a}$$

$$f_T^{2,\text{dip}} = \sum_{T_i,L_r,T_r} \jmath k_2 n_2^m R_m^{\perp} e^{-\jmath(k_1^m + k_2 \tan\varphi_r) x_1^S}, \tag{12b}$$

where factors $R_m^{\perp}$ represent the reflection coefficients of the incident shear wave at the free surface.[38]

D. Directivity function of a buried line source of expansion

By applying the superposition principle [Eq. (3)], the directivity functions f_L^S and f_T^S of a single buried line source of expansion of unit amplitude in the half-space are obtained,

$$f_L^S(\theta, x_1^S) = \sum_{L_i,L_r,T_r} R_m^{\parallel}(\theta) \jmath \mathbf{k}_m(\theta) \cdot \mathbf{n}_m(\theta) \cdots e^{-\jmath[k_1^m(\theta) + k_2(\theta)\tan\varphi_r] x_1^S}, \tag{13a}$$

$$f_T^S(\theta, x_1^S) = \sum_{T_i,L_r,T_r} R_m^{\perp}(\theta) \jmath \mathbf{k}_m(\theta) \cdot \mathbf{n}_m(\theta) \cdots e^{-\jmath[k_1^m(\theta) + k_2(\theta)\tan\varphi_r] x_1^S}. \tag{13b}$$

These expressions contain the scalar product between the wave vectors and polarization vectors of each incident and reflected waves. However, in an isotropic material and in the case of a shear wave, this product is zero, $\mathbf{k}_{T_i} \cdot \mathbf{n}_{T_i} = \mathbf{k}_{T_r} \cdot \mathbf{n}_{T_r} = 0$, which leads to the simplification

$$f_T^S(\theta, x_1^S) = R_{L_r}^{\perp}(\theta) \jmath \mathbf{k}_{L_r}(\theta) \cdot \mathbf{n}_{L_r}(\theta) \cdots e^{-\jmath[k_1^{L_r}(\theta) + k_2(\theta)\tan\varphi_r] x_1^S}. \tag{14}$$

This observation shows that only waves generating deformations associated with a change in volume contribute to the directivity of a buried source of expansion.[36] Thus in an isotropic medium, a buried source of expansion can generate shear waves only in the presence of an interface where mode conversion of compressional to shear waves can occur.

E. Directivity function of a tilted buried source layer

As mentioned previously, the buried source layer has been decomposed into a sum of buried line sources of expansion. To complete the calculation of the directivity functions for a buried source layer, the last step is to introduce $f_L^S(\theta, x_1^S)$ and $f_T^S(\theta, x_1^S)$, Eqs. (13a) and (14), into Eq. (5), and to integrate over the buried sources of expansion. The directivity functions of a tilted buried source layer are thereby obtained,

$$f_L^{\text{OP}}(\theta) = \sum_{L_i,L_r} \frac{\beta(\varphi_r) R_m^{\parallel}(\theta) \jmath \mathbf{k}_m(\theta) \cdot \mathbf{n}_m(\theta)}{\beta(\varphi_r) + \jmath[k_1^m(\theta) + k_2(\theta)\tan\varphi_r]}, \tag{15a}$$

$$f_T^{\text{OP}}(\theta) = \frac{\beta(\varphi_r) R_{L_r}^{\parallel}(\theta) \jmath \mathbf{k}_{L_r}(\theta) \cdot \mathbf{n}_{L_r}(\theta)}{\beta(\varphi_r) + \jmath[k_1^{L_r}(\theta) + k_2(\theta)\tan\varphi_r]}. \tag{15b}$$

Note the expressions of f_L^{OP} and f_T^{OP}, Eq. (15), depend on the angle of refraction φ_r of the laser beam.

To summarize this section, we have presented a method for calculating the analytical expressions of the directivity functions of compressional and shear waves generated by a tilted buried source layer where optical penetration depth as well as the angle of incidence of the laser beam are both taken into account. Let us now analyze these results for a simple illustrative case.

IV. CONTRIBUTION OF COMPRESSIONAL WAVES TO THE DIRECTIVITY OF SHEAR WAVES IN THE CASE OF A SINGLE BURIED LINE SOURCE OF EXPANSION

Before analyzing the directivity patterns of a tilted buried source layer, we propose to investigate first the case of a single buried line source of expansion. This simpler source allows one to examine the particular case of the shear-wave

Redistribution subject to ASA license or copyright; see http://acousticalsociety.org/content/terms. Download to IP: 134.157.146.58 On: Fri, 10 Jan 2014 11:32:51

generation that is exclusively due to mode conversion of the generated compressional waves at the free surface of the half-space. We plot in Fig. 2(a) the directivity functions $f_T^S(\theta, x_1^S)$ [Eq. (14)] vs angle of observation θ for a single line source of expansion of unit amplitude buried at a distance $x_1^S = 1/\beta$ below the surface of the half-space. The pulsation used in the calculations is $\omega = \beta c_T$, with c_T the shear-wave celerity. This pulsation corresponds to a ratio $k_T/\beta = 1$, where k_T is the wave number of shear waves. Two zones separated by the direction of maximum generation of shear waves appear in Fig. 2(a): the central zone containing the two primary lobes and side zones containing the lateral lobes. The origin of these zones together with the particular case of the direction of the maximum generation is now discussed by considering mode conversion of compressional waves. Mode conversions of three different types (skimming, evanescent, or bulk) of compressional waves are investigated.

To discuss mode conversions at a free surface, it is convenient to consider the phase slowness as shown in Fig. 2(b). Since the medium is isotropic, the phase slowness of compressional waves (respectively, shear waves), of celerity c_L (respectively, c_T), define an arc of radius $1/c_L$ (respectively, $1/c_T$) in the plane $(|\mathrm{Re}(k_1/\omega)|, |k_2/\omega|)$, where $\mathrm{Re}(\cdot)$ represents the real part of a complex number. Owing to Snell's law, the projections along the free surface of the wave vectors of incident and reflected waves are both equal to k_2 [vertical dotted lines in Fig. 2(b)]. In the particular case where $k_2/\omega = 1/c_L$, which defines the critical angle θ_{cr},

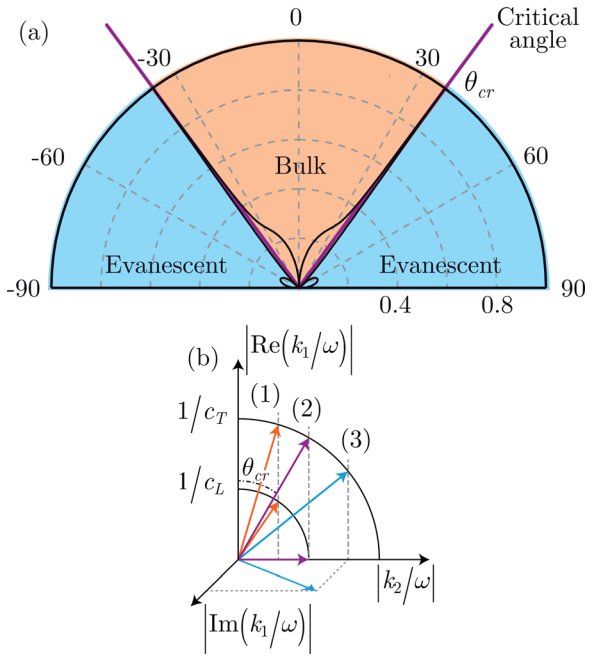


FIG. 2. (Color online) (a) Directivity pattern for shear waves of a buried source of expansion at a distance $x_1^S = 1/\beta$ to the surface. The pulsation used in the calculations is $\omega = \beta c_T$, corresponding to a ratio $k_T/\beta = 1$. (b) Phase slowness in an isotropic medium and representations of wave vectors of the incident shear wave and the reflected compressional wave depending on the values of the angle of incidence θ_i of the shear waves: (1) $\theta_i < \theta_{\mathrm{cr}}$, (2) $\theta_i = \theta_{\mathrm{cr}}$, and (3) $\theta_i > \theta_{\mathrm{cr}}$.

$$\theta_{\mathrm{cr}} = \sin^{-1}\left(\frac{c_T}{c_L}\right), \tag{16}$$

compressional waves are skimming waves propagating along the free surface without decay in amplitude with respect to depth, case (2) in Fig. 2(b). In Fig. 2(a), c_L and c_T are in a ratio such that the critical angle is about 35°. If $k_2/\omega < 1/c_L$, i.e., $\theta < \theta_{\mathrm{cr}}$ [case (1) in Fig. 2(b)], both compressional and shear waves are bulk waves. On the contrary, if $k_2/\omega > 1/c_L$, i.e., $\theta > \theta_{\mathrm{cr}}$ [case (3) in Fig. 2(b)], compressional waves are evanescent waves that propagate along the free surface and decay exponentially with respect to depth.

Accordingly, it is clear that shear waves generated in directions strictly between $-\theta_{\mathrm{cr}}$ and θ_{cr} [case (1)], which correspond to the two primary lobes in the central zone in Fig. 2(a), originate from the mode conversion at the free surface of bulk compressional waves generated by the source of expansion. Since there is no mode conversion of compressional waves at normal incidence, there is no contribution to the directivity of shear wave at $\theta = 0°$. The shear waves generated in the directions $-\theta_{\mathrm{cr}}$ and θ_{cr} [case (2)], which correspond to the directions of maximum generation, originate from the mode conversion of the skimming compressional waves. These shear waves are called head waves in the remainder. Finally the shear waves generated in directions below $-\theta_{\mathrm{cr}}$ or above θ_{cr} [case (3)], which correspond to the lateral lobes in Fig. 2(a), are a result of mode conversion of the evanescent compressional waves.

In contrast to the standard analysis of directivity patterns for surface sources, we have identified an additional contribution to the generation of shear waves that appears in the case of a buried line source of expansion. This analysis, and in particular the contribution of evanescent compressional waves, plays a pivotal role in the understanding of the directivity of a buried source layer.

V. DIRECTIVITY PATTERNS OF A NORMAL BURIED SOURCE LAYER

The method described in Sec. III. to calculate the directivity functions is now used to analyze the radiation of a normal buried source layer. The case of semi-transparent materials is considered. The patterns obtained with the present method are analyzed and compared to those found in the literature for an acoustic source resulting from the absorption of an electromagnetic wave at normal incidence.

To analyze the influence of the optical penetration on directivity patterns, we model a neutral glass with values of the ratio k_L/β identical to those found in the literature, where k_L is the wave number of compressional waves.[34] Figure 3 shows directivity patterns for compressional waves plotted for a ratio k_L/β equal to (a) 0.01, (b) 0.2, (c) 0.3, (d) 0.5, (e) 1, (f) 2, (g) 3, (h) 5, and (i) 10. All diagrams are normalized by the maximum of curve (a). We observe an excellent agreement with the directivity patterns reported in the literature for all diagrams,[34] thus confirming the validity of our calculations.

When $k_L/\beta \ll 1$, curve (a) in Fig. 3, the directivity of compressional waves is identical to that of a thermoelastic

Redistribution subject to ASA license or copyright; see http://acousticalsociety.org/content/terms. Download to IP: 134.157.146.58 On: Fri, 10 Jan 2014 11:32:51

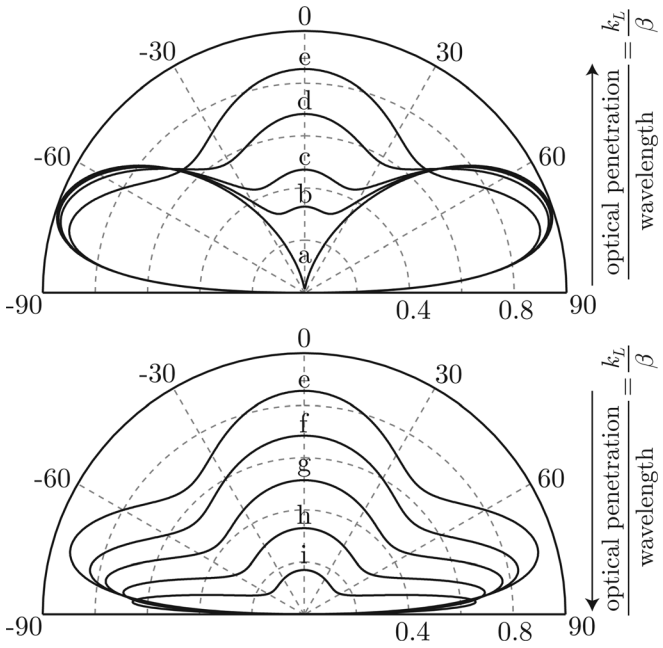


FIG. 3. Directivity patterns for compressional waves for a sample of neutral glass plotted for k_L/β equal to (a) 0.01, (b) 0.2, (c) 0.3, (d) 0.5, (e) 1, (f) 2, (g) 3, (h) 5, and (i) 10.

surface dipole source.[36] Thus, taking into account the optical penetration has little influence on waves of very large wavelength compared to the optical penetration depth. However, as k_L/β increases, an additional contribution appears for $\theta = 0°$ [curves (b)–(e) in Fig. 3]: increasing optical penetration increases the directivity of compressional waves. Finally, when the ratio is greater than 1, the shape of the directivity pattern remains the same and its amplitude decreases with increasing k_L/β due to a decrease in generation efficiency for waves of wavelengths smaller than the optical penetration depth. The directivity of compressional waves is thus increasingly influenced by the penetration of the laser beam as their wavelength becomes increasingly close to the optical penetration depth.

We plot in Fig. 4 the directivity patterns of shear waves for the following three values of the ratio k_T/β: (a) 0.01, (b) 1, and (c) 2π. The directivities presented in Ref. 34 can be reproduced perfectly by our calculations with an angular step of 1°. Each curve is normalized by its maximum in this case. However, with such a rough angular step, the directions associated to the head waves are not calculated precisely, and the maximum value for the normalization changes from one curve to another. The patterns therefore seem not to vary much.[34] This analysis can be misleading, and a more precise angular step is necessary to resolve the sharp head wave pattern.

For a more detailed analysis, the calculations are now carried out with an angular step of 1/6°, for $k_T/\beta = 0.01$ (solid line in Fig. 5) and $k_T/\beta = 1$ (dashed line in Fig. 5). In this case, both diagrams are normalized by the maximum of the solid curve. We observe that the amplitude of shear waves propagating in directions contained in the cone of half top angle θ_{cr} decrease with increasing wavelength. As demonstrated in Sec. IV, these waves are associated with the

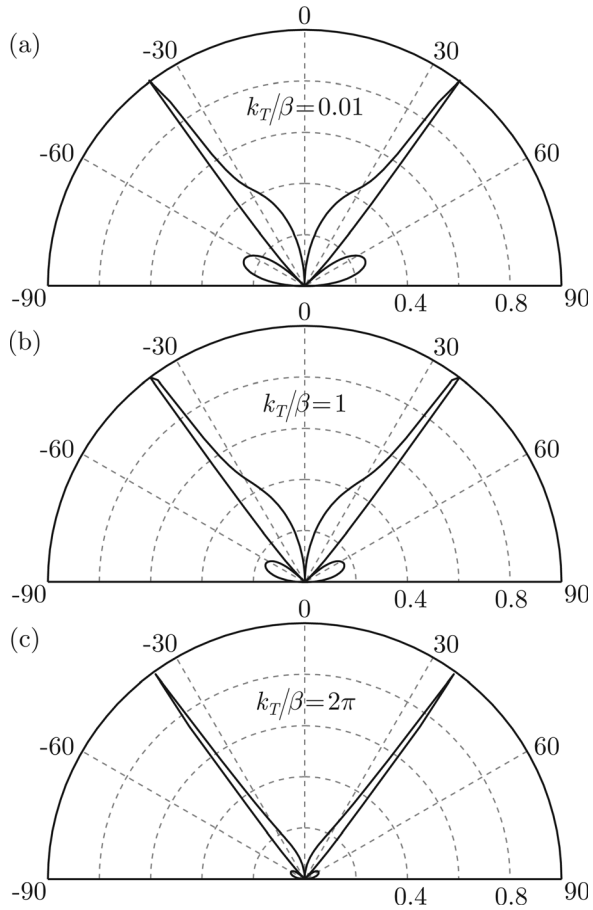


FIG. 4. Directivity patterns for shear waves for a sample of neutral glass plotted for k_T/β equal to (a) 0.01, (b) 1, and (c) 2π.

mode conversion of bulk compressional waves. The observed changes in the directivity of the shear waves within the cone must thus be discussed together with those in the directivity patterns of the bulk compressional waves (Fig. 3) considered for the whole angular sector. For a given ratio k_T/β, the equivalent ratio k_L/β to consider for comparison is obtained by the following equation:

$$\frac{k_L}{\beta} = \frac{c_T}{c_L}\frac{k_T}{\beta}. \tag{17}$$

From Eq. (17), values of $k_T/\beta = 0.01$ and 1 considered here correspond to $k_L/\beta \approx 0.01$ and 0.5, respectively. We thus

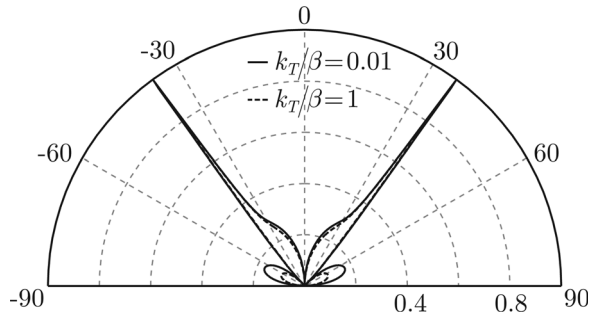


FIG. 5. Directivity patterns for shear waves for a sample of neutral glass for k_T/β equal to 0.01 (solid) and 1 (dashed).

Redistribution subject to ASA license or copyright; see http://acousticalsociety.org/content/terms. Download to IP: 134.157.146.58 On: Fri, 10 Jan 2014 11:32:51

compare solid and dotted lines in Fig. 5 to the directivity patterns of Figs. 3(a) and 3(d), respectively. For compressional waves, Figs. 3(a)–3(d) shows that the area of the directivity pattern increases as k_L/β increases. Owing to energy conservation, such an increase of compressional-wave amplitude for all angles is balanced by a decrease in the amplitude of shear waves observed for $|\theta| < \theta_{cr}$, Fig. 5. Note that the amplitude of the head waves remains approximately the same in this range of values for k_T/β.

A more pronounced decrease of the shear-wave amplitude with increasing penetration depth is visible on the lateral lobes in Fig. 5. As previously mentioned, shear waves associated to these lobes originate from evanescent compressional waves. Evanescent waves propagate along the free-surface, and are characterized by an exponential decrease of their in-depth amplitude. The increase in optical penetration $1/\beta$ therefore spatially filters the evanescent waves with an in-depth amplitude that decays faster than $1/\beta$. This results in the observed decrease of the amplitude of the lateral lobes.

By identifying the different contributions to shear wave directivity, we have explained the effect of the optical penetration depth on the directivity of a normal buried source layer for both compressional and shear waves. Section VI is now dedicated to the investigation of effects of the obliquity of the volume acoustic source.

VI. DIRECTIVITY PATTERNS OF A TILTED BURIED SOURCE LAYER

In strongly absorbing materials, such as metals, the characteristic acoustic pulsation ω_c is imposed by the laser duration τ. In order to analyze the influence of the obliquity both theoretically and experimentally, we choose an actual sample with an optical penetration depth $1/\beta \gg \tau c_L$. In this configuration, $\omega_c = \beta c_L$ is imposed by the optical penetration depth, and not by the laser pulse duration. The sample is thus a plate made of Schott NG1 glass. The relevant physical properties[39] are summarized in Table I. The effects of the obliquity of the acoustic source are first analyzed for compressional-wave directivity patterns and then for shear-wave directivity patterns.

In contrast to Sec. V, the buried source layer forms a positive angle φ_r with the normal to the surface of the sample, owing to the refraction of the laser beam. Figures 6(a) and 6(b) show the change in the directivity of compressional waves for a ratio $k_L/\beta(\varphi_i) = 1$ and 2π, respectively. The directivities are plotted for two values of the angle of incidence of the laser beam φ_i: (i) 0° and (ii) 45°. The corresponding angles of refraction φ_r are (i) 0° and (ii) 28°, respectively. Each curve is normalized to its maximum amplitude. As expected, since ω_c is imposed by the optical penetration depth, the effect of the obliquity of the acoustic source is more pronounced for compressional waves of wavelength equal to the optical penetration depth [$k_L/\beta = 2\pi$, Fig. 6(b)] than for compressional waves of larger wavelength [$k_L/\beta = 1$, Fig. 6(a)].

TABLE I. Mechanical and optical (at 1064 nm) properties of the Schott NG1 glass. The density ρ and the thickness h are measured. The stiffness coefficients $C_{11} = \rho V_C^2$ and $C_{66} = \rho V_S^2$ are calculated from the measured compressional-wave and shear-wave velocities: V_C and V_S, respectively.

	Value
Stiffness coefficient C_{11} (GPa)	66.91
Stiffness coefficient C_{66} (GPa)	23.4
Density ρ (g cm^{-3})	2.443
Optical penetration depth[a] $1/\beta$ (0°) [μm]	226
Refractive index[a] n'	1.51
Absorption coefficient[a] n''	3.74×10^{-4}

[a]Reference 39.

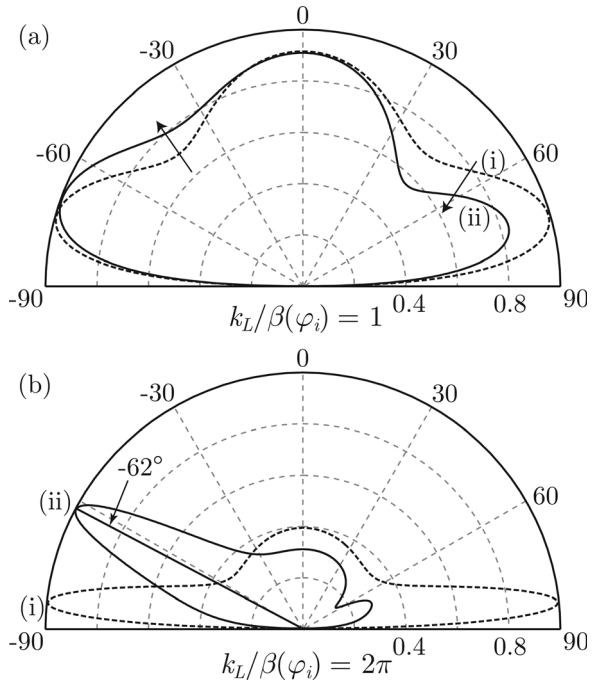


FIG. 6. Directivity patterns for compressional waves in the Schott NG1 glass for (b) $k_L/\beta(\varphi_i) = 1$ and (b) 2π. In both cases the angle of incidence is φ_i: (i) 0° and (ii) 45°.

In Fig. 6(b), a striking feature of the directivity pattern for the oblique buried source layer is that the generation of the compressional waves is more intense in two particular directions. For an angle of incidence of the laser beam of 45°, corresponding to an angle of refraction of 28°, the direction of the highest compressional-wave amplitude is −62°. This direction corresponds exactly to the direction normal to the direction of refraction. Another lobe oriented in the 62° direction also appears, but with a much smaller amplitude. Indeed, since the lateral dimension of the expansion source is neglected in the present model, the compressional waves are preferentially generated in the direction normal to the source, i.e., in the direction normal to the direction of refraction. Yet, to explain why the generation is more intense for $\theta < 0$, that is in the diagram area opposite to that of the source, a more detailed analysis of mode conversion is necessary.

The −62° lobe originates from compressional waves propagating freely toward the bulk of the material. Conversely, the 62° lobe results from compressional waves propagating toward the surface of the half-space, that reflect without mode conversion. However, shear waves are also

Redistribution subject to ASA license or copyright; see http://acousticalsociety.org/content/terms. Download to IP: 134.157.146.58 On: Fri, 10 Jan 2014 11:32:51

generated by mode conversion at this surface. A transfer of mechanical energy from compressional to shear waves thus explains why the amplitude of the 62° lobe is smaller.

To confirm this analysis, consider now the directivity of shear waves. The same angles of incidence are considered and the ratio k_T/β (φ_i) is equal to 2π in Fig. 7. Again, each curve is normalized by its maximum amplitude. Similarly to compressional waves in Fig. 6(a), the ratio $k_T/\beta(\varphi_i)=1$ would have shown that the effects of the obliquity on the directivity of shear waves are small where the wavelength is larger than the optical penetration depth.

In Fig. 7, the directions of the two maxima of amplitude on the shear-wave directivity patterns do not change with the obliquity and remain symmetrical. As identified in Sec. IV, these maxima directions correspond to head waves generated at the critical angle θ_{cr}, determined solely by the mechanical properties of the propagating medium. This indicates that the directivity of head waves is not influenced by the loss of symmetry of the source.

The small lateral lobes on the shear-wave directivity patterns, originating from evanescent compressional waves, also remain symmetrical when the angle of incidence is changed (Fig. 7). However, their magnitude increases symmetrically with increasing angle of incidence. Indeed, as shown in Sec. II, the effective optical penetration depth decreases as the angle of incidence increases.[35] The electromagnetic energy deposition is thus concentrated on a volume increasingly close to the surface. The generation of evanescent waves with small wavelengths is thus favored.

The most striking feature owing to mode conversion of bulk compressional waves is that the obliquity leads to the formation of a new central lobe indicated by a line in Fig. 7(b). Consider the angle θ_T formed by the propagation direction of the reflected shear waves with the normal to the surface of the half-space,

$$\theta_T = \sin^{-1}\left[\frac{c_T}{c_L}\sin\left(\frac{\pi}{2}-\varphi_r\right)\right], \tag{18}$$

given by Snell's law. For $\varphi_r=28°$ (corresponding to $\varphi_i=45°$), Eq. (18) leads to an angle of $\theta_T=31°$ corresponding exactly to the position of the new lobe. This shows that when the angle of refraction becomes smaller than the critical angle, a new favored direction for shear wave generation appears. Equation (18) explicitly relates the favored direction for the generation of acoustic shear waves to the direction of light refraction.

We have seen that the amplitude of shear waves originating from evanescent compressional wave increases with increasing angle of incidence. Moreover, we have demonstrated the existence of a favored direction θ_T for enhanced shear-wave generation. This direction can be controlled merely by tuning the incident laser angle, see, for instance, the lobe at $\theta_T=31°$ for $\varphi_i=45°$. To confirm this ability to steer shear wave generation, comparisons with experimental results are now proposed.

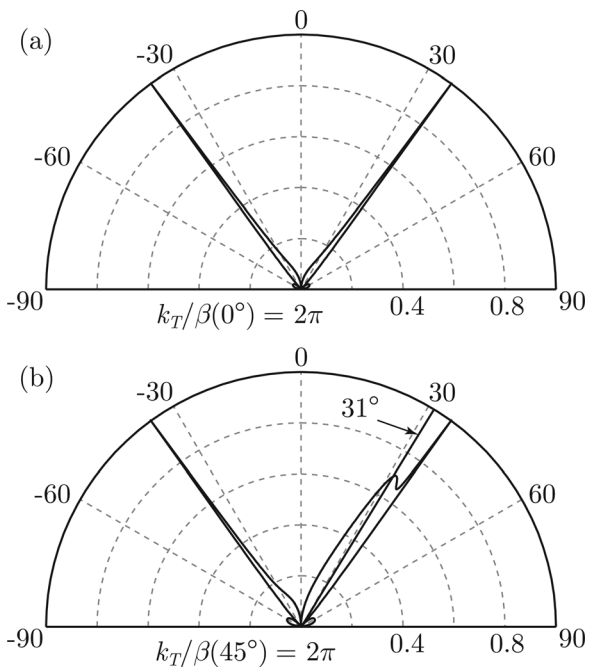


FIG. 7. Directivity patterns for shear waves for the Schott NG1 glass for the ratio $k_T/\beta(\varphi_i)$ equal to 2π with changes in the angle of incidence φ_i. The values of φ_i are (a) 0° and (b) 45°.

VII. COMPARISONS OF CALCULATED DIRECTIVITY PATTERNS WITH EXPERIMENTAL RESULTS

The experimental setup used to measure the amplitudes of compressional and shear waves with respect to the angle of observation is first introduced. The experimental results are then analyzed and finally compared to calculated directivity patterns.

A. Measurement of pseudo-directivity patterns

A Q-switched Nd:YAG laser delivering 8 ns pulses is focused to a line of width $\sim$100 μm and length $\sim$3 cm at the front surface ($x_1=0$) of a NG1 Schott glass plate. The optical penetration depth of about $1/\beta=230$ μm dominates the frequency content of the acoustic waves and the pulse duration has little influence, as explained previously. Owing to the finite lateral dimension of the source, the thermoelastic expansion generates a diffracted acoustic field in the plate. Successive reflections with mode conversion at the plate boundaries create compressional and shear echoes. A continuous laser interferometer focused to a spot of radius $\sim$100 μm is used to measure the normal component of the displacement of the rear surface of the plate ($x_1=h$). The laser source to detector position is scanned along $\mathbf{x}_2$ using a motorized stage with a step of angle of observation of 2° and for both normal and $\varphi_i=45°$ laser incidences. Note that the angular step does not allow measurement of the very narrow peak of maximum amplitude associated to the head waves in the critical angle θ_{cr} direction.

The amplitudes of the compressional and shear acoustic echoes are plotted in polar coordinates vs θ for both normal and oblique configurations in Fig. 8. The case of normal incidence is represented in Figs. 8(a) and 8(b) and the case of $\varphi_i=45°$ is represented in Figs. 8(c) and 8(d). In both normal and oblique cases, the amplitudes are normalized by the

Redistribution subject to ASA license or copyright; see http://acousticalsociety.org/content/terms. Download to IP: 134.157.146.58 On: Fri, 10 Jan 2014 11:32:51

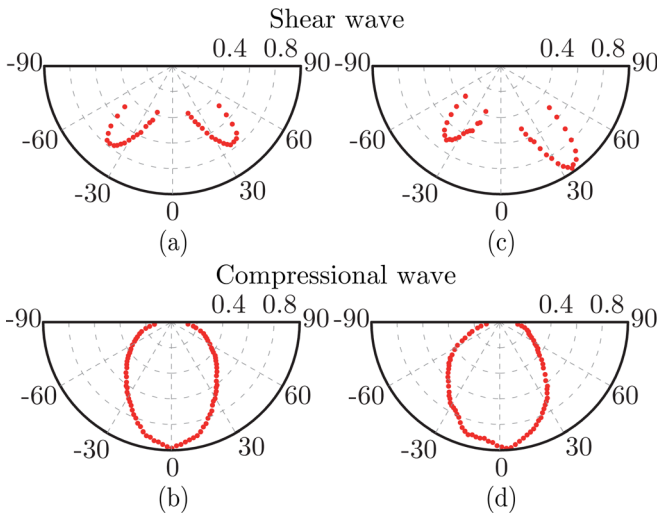


FIG. 8. (Color online) Amplitudes of (a) the shear waves and (b) the compressional waves for a normal buried source layer and amplitudes of (c) the shear waves and (d) the compressional waves for a tilted buried source layer ($\varphi_i = 45°$) plotted vs θ for experimental results.

compressional wave amplitude for $\theta = 0°$. The details of the experiment are given in Ref. 35.

The experimental polar diagrams (Fig. 8), so-called pseudo-directivity patterns, are reminiscent of the directivity patterns presented in Secs. V and VI. However, there are three major differences between the two types of patterns. (i) The directivity patterns are calculated for a given frequency. The pseudo-directivity diagrams are obtained from temporal signals, i.e., the whole signal spectrum is taken into account at each point. It will be shown in the remainder to have a small influence on the difference between pseudo-directivity and directivity patterns compared to the other transformations discussed in this section. (ii) In the case of the directivity patterns for compressional waves, the reported amplitudes correspond to the amplitude of the displacement in the direction of observation, and in the case of the directivity patterns for shear waves, the reported amplitudes correspond to the amplitude of the displacement in the direction normal to the direction of observation. The pseudo-directivity patterns give access to the component of the displacement in a direction normal to the surface of the plate. Moreover, the points of observation are distributed on a semi-circle for the directivity patterns and along a plane surface for the pseudo-directivity patterns, meaning that in the latter case the distance from the source is not constant. (iii) The measurement of the amplitudes for the pseudo-directivity is performed at a free surface, whereas the amplitudes are measured in the bulk of a half-space for the directivity. To compare both types of patterns, we transform the directivity patterns calculated at a characteristic frequency for equivalent measurement conditions to compensate for (ii) and (iii).

B. Transformation of the directivity patterns

Consider Fig. 9 for discussion. The quarter-circle of radius h, where h is the thickness of the plate, describes the location of the points of observation in the case of the directivity patterns. Point C is the point of observation belonging

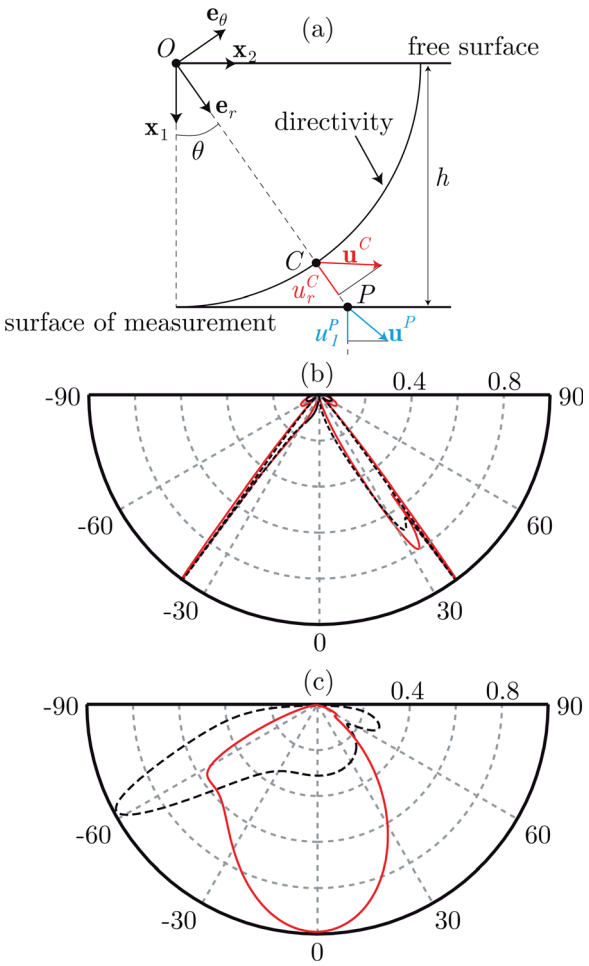


FIG. 9. (Color online) (a) Diagram of the difference in orientation and attenuation of the measured displacements to plot the pattern of directivity or that of pseudo-directivity of compressional waves. Directivity patterns (dotted lines) and transformed directivity patterns (solid lines) for (b) the shear waves and (c) the compressional waves for a tilted buried source layer ($\varphi_i = 45°$).

to the quarter-circle for the direction of observation θ. The points of observation in the case of the pseudo-directivity patterns are distributed on the rear surface of the plate, Fig. 9(a). Point P represents the point of observation belonging to the rear surface of the plate for the same direction of observation θ. The transformations accounting for the differences in the direction of measured displacements and in the distances covered by the waves at the time of their measurement simply lead to a multiplication of the directivity functions by a factor $K_L(\theta)$ [respectively, $K_T(\theta)$] for compressional waves (respectively, shear waves). The details of their calculation are reported in the Appendix.

For the directivity patterns, the amplitudes are calculated at point C in the bulk of the half-space, and are therefore only due to the incident wave. For the pseudo-directivity, the amplitudes measured at a free surface at point P are a combination of the incident wave and of the waves reflected with and without mode conversion. To compensate for this difference, it is necessary to introduce the reflection coefficients at the rear surface.[40] To do so, we introduce a virtual secondary source located at the rear surface. We first describe the transformation to apply in the case of the

Redistribution subject to ASA license or copyright; see http://acousticalsociety.org/content/terms. Download to IP: 134.157.146.58 On: Fri, 10 Jan 2014 11:32:51

directivity function of compressional waves f_L^{OP} [Eq. (15a)]. Shear waves will be analyzed later.

As explained previously, the normal displacement at point P is caused by an incident compressional wave that is reflected at the rear surface ($x_1 = h$) and that gives rise to a compressional wave and to a shear wave owing to mode conversion. To model these reflections, the solid medium can be described as a half-space $x_1 \leq h$. The incident compressional plane wave impinging on the rear surface at point P with an angle θ is considered to be generated by a single force buried far from the surface and applied along direction θ. In this configuration, the calculation of the normal displacement at point P caused by the incident and reflected waves corresponds exactly to the reciprocal problem one would have to solve in order to obtain the directivity function f_L^{sec} for compressional waves generated by a virtual secondary source located at point P. Since we measure the normal displacements at the rear surface, this secondary source is a monopole oriented along $\mathbf{x}_1$ and located at the rear surface. Function f_L^{sec} can thus be obtained by solving a reciprocal problem such as the one described in Sec. III.

The amplitude of the normal displacement at point P on the rear surface generated by the incident compressional wave of amplitude u_r^C is then obtained by the product $u_r^C f_L^{sec}(\theta)$ in order to take into account the reflections occurring at the free surface. In other words, to transform the directivity pattern in order to take into account the measurement at a free surface, the directivity function f_L^{OP}, calculated in the bulk of the material, has to be multiplied by the directivity function f_L^{sec} of the secondary source.

Finally, the directivity function f_L^{OP} [Eq. (15a)] has to be multiplied by $K_L(\theta)\, f_L^{sec}(\theta)$, where $K_L(\theta)$ is expressed in the Appendix, in order to transform the directivity and to compare the pseudo-directivity with the transformed directivity of the compressional waves. Similarly, it can be shown that to transform the directivity of the shear waves, the directivity function f_T^{OP} [Eq. (15b)] has to be multiplied by $K_T(\theta)\, f_T^{sec}(\theta)$, where $K_T(\theta)$ is expressed in the Appendix and the function f_T^{sec} is the directivity function of the shear waves for a monopole oriented along $\mathbf{x}_1$ and applied at the free surface.

In Figs. 9(b) and 9(c), the directivity patterns (dotted lines) and the transformed directivity patterns (solid lines) of a tilted buried source layer for $\varphi_i = 45°$ are plotted for the shear and the compressional waves, respectively. These patterns are calculated at a characteristic frequency ω_c such that the wavelength of each type of waves is equal to the optical penetration depth, i.e., $\omega_c = 2\pi\beta c_T$ for shear waves and $\omega_c = 2\pi\beta c_L$ for compressional waves.

In Fig. 9(b), the transformations made to the directivity of the shear waves increase the magnitude of the new favored generation direction in the area where the volume acoustic source is located. The direction associated to the sharp maximum of shear-wave generation remains that of the critical angle associated to the head waves. Figure 9(c) shows that even for the frequency where the obliquity effects on the directivity patterns are theoretically important, the asymmetry of the pattern for the compressional waves is moderate once transformed. The measurement at the rear surface of the plate masks the favored generation enlightened by the directivity patterns calculated in the bulk of the material. This observation is valid for all lower frequencies since the obliquity effects become even less noticeable.

C. Comparison of pseudo-directivity with transformed directivity patterns

In Fig. 8 representing the measured pseudo-directivity patterns, a loss of symmetry appears for both shear and compressional waves where the incidence of the laser beam is oblique. These experimental results are compared with the transformed directivity patterns presented in Sec. VII B.

In the case of shear waves in Fig. 8(c), the increase of the amplitude of the lobe in the area where the source is located is well described by the new favored direction in the direction of 31° [Eq. (18)], noteworthy in the transformed directivity patterns in Fig. 9(b). The measured pseudo-directivity pattern in Fig. 8(d) is also well reproduced by the transformed directivity patterns in Fig. 9(c), thus underscoring that the proposed transformation of directivity patterns allows very good predictions of acoustic beam steering.

To summarize, a comparison of the measured pseudo-directivity patterns with the calculated directivity patterns has been proposed. For the first time, a virtual secondary source has been introduced to model the detection at a free plane surface. The rear surface is shown to mask the favored direction of generation. Despite this filter, the acoustic beam steering with light refraction for compressional and especially shear waves was demonstrated. In the future, it would be interesting to use this ability for non-destructive laser-ultrasonic inspection with a tunable angle of incidence of the laser.

VIII. CONCLUSIONS

We have presented a method for calculating the analytical expressions of the directivity functions of compressional and shear waves generated by an acoustic source distributed in the volume of the sample. These calculations have been applied to the case of the thermoelastic generation by a volume absorption of an electromagnetic wave at oblique incidence.

The origin of different lobes appearing on the directivity patterns of compressional and shear waves has been identified. In contrast to the standard analysis of directivity patterns for surface sources, we have revealed an additional contribution of evanescent compressional waves to the generation of shear waves that appears in the case of a buried source of expansion. This analysis plays a pivotal role in the understanding of the directivity of volume sources.

We have shown that the contribution of evanescent waves increases with increasing angle of incidence. Moreover, we have demonstrated the existence of a favored direction for enhanced shear-wave generation. This favored direction is controlled by tuning the angle of incidence of the laser beam. Since the direction of maximum generation has been shown to be normal to the direction of refraction, the amplitude of bulk compressional waves can be tuned similarly by adjusting laser incidence.

Redistribution subject to ASA license or copyright; see http://acousticalsociety.org/content/terms. Download to IP: 134.157.146.58 On: Fri, 10 Jan 2014 11:32:51

The ability to steer acoustic wave by light refraction was then demonstrated with an experiment performed with a plate. A prediction of the measured pseudo-directivity patterns was proposed by introducing a virtual secondary source to model the detection at a free plane surface.

Despite the fact that the rear free surface is shown to mask part of the actual steering, a strong asymmetry of the pseudo-directivity pattern of shear waves is demonstrated. These results, together with the ability to modulate bulk-wave amplitudes and to select the directivity of volume sources, suggest important applications in non-destructive testing and imaging.

APPENDIX

The differences in the directions of measured displacements and in the distances over which the waves have traveled at the time of their measurement are considered in this appendix. The transformation factors to apply to the directivity patterns in order to correct these differences are presented.

As an example, consider the directivity pattern and the pseudo-directivity pattern of the compressional waves. In Fig. 9(a), $\mathbf{u}^C$ is the displacement vector at the point C. The projection u_r^C of $\mathbf{u}^C$ on the direction $\mathbf{e}_r$ corresponds to the amplitude reported on the directivity pattern of the compressional waves in the direction of observation θ. $\mathbf{u}^P$ is the displacement vector at the point P. The projection u_1^P of $\mathbf{u}^P$ on the direction $\mathbf{x}_1$ corresponds to the amplitude reported on the pseudo-directivity pattern of the compressional waves in the direction of observation θ. By multiplying u_r^C by $\cos\theta$, the amplitude of the compressional wave at point C are transformed as if it was measured along $\mathbf{x}_1$ rather than along $\mathbf{e}_r$.

In addition, the variation in the distance traveled by the wave between points P and C should be considered. Indeed, the amplitude of the cylindrical waves measured far from the source decays in $1/\sqrt{r}$, where r is the distance between the source and the point of observation. Waves reaching points of observation on the quarter-circle have the same attenuation $1/\sqrt{h}$. This attenuation factor does not depend on the angle of observation θ, and consequently does not appear in the directivity functions. On the contrary, for the pseudodirectivity, the waves are detected after they have traveled a longer distance $h/\cos\theta$ that depends on θ. It is thus necessary to multiply the amplitude u_r^C by $\sqrt{\cos\theta}$ to compensate for this change in attenuation.

Finally, the transformation factor accounting for differences in the directions of measured displacements and in the distances for wave propagation from the source to the point of observation is $K_L(\theta) = (\cos\theta)^{3/2}$. Similarly, it can be shown that in the case of shear waves, the transformation factor is $K_T(\theta) = |\sqrt{\cos\theta}\sin\theta|$.

[1]B. Temelkuran, M. Bayindir, E. Ozbay, R. Biswas, M. M. Sigalas, G. Tuttle, and K. M. Ho, "Photonic crystal-based resonant antenna with a very high directivity," J. Appl. Phys. **87**, 603–605 (2000).

[2]H. J. Lezec, A. Degiron, E. Devaux, R. A. Linke, L. Martin-Moreno, F. J. GarciaVidal, and T. W. Ebbesen, "Beaming light from a subwavelength aperture," Science **297**, 820–822 (2002).

[3]J. Reijniers, D. Vanderelst, and H. Peremans, "Morphology-induced information transfer in bat sonar," Phys. Rev. Lett. **105**, 148701 (2010).

[4]A. McAlpine, A. P. Daymond-King, and A. J. Kempton, "Sound radiation from a flanged inclined duct," J. Acoust. Soc. Am. **132**, 3637–3646 (2012).

[5]P. Roux, B. D. Cornuelle, W. A. Kuperman, and W. S. Hodgkiss, "The structure of raylike arrivals in a shallow-water waveguide," J. Acoust. Soc. Am. **124**, 3430–3439 (2008).

[6]B. De Cacqueray, P. Roux, M. Campillo, S. Catheline, and P. Boue, "Elastic-wave identification and extraction through array processing: An experimental investigation at the laboratory scale," J. Appl. Geophys. **74**, 81–88 (2011).

[7]A. Macovski, "Ultrasonic imaging using arrays," Proc. IEEE **67**, 484–495 (1979).

[8]O. T. Von Ramm and S. W. Smith, "Beam steering with linear arrays," IEEE Trans. Biomed. Eng. **30**, 438–452 (1983).

[9]S. W. Smith, H. G. Pavy, Jr., and O. T. von Ramm, "High-speed ultrasound volumetric imaging system—I: Transducer design and beam steering," IEEE Trans. Ultrason. Ferroelectr. Freq. Control **38**, 100–108 (1991).

[10]J. Li and J. L. Rose, "Implementing guided wave mode control by use of a phased transducer array," IEEE Trans. Ultrason. Ferroelectr. Freq. Control **48**, 761–768 (2001).

[11]P. D. Wilcox, "Omni-directional guided wave transducer arrays for the rapid inspection of large areas of plate structures," IEEE Trans. Ultrason. Ferroelectr. Freq. Control **50**, 699–709 (2003).

[12]K. Hynynen, G. T. Clement, N. McDannold, N. Vykhodtseva, R. King, P. J. White, S. Vitek, and F. A. Jolesz, "500-element ultrasound phased array system for noninvasive focal surgery of the brain: A preliminary rabbit study with ex vivo human skulls," Magn. Reson. Med. **52**, 100–107 (2004).

[13]Y. Berthelot and I. Busch-Vishniac, "Thermoacoustic radiation of sound by a moving laser source," J. Acoust. Soc. Am. **81**, 317–327 (1987).

[14]R. K. Ing, M. Fink, and F. Gires, "Directivity patterns of a moving thermoelastic source in solid media," IEEE Trans. Ultrason. Ferroelectr. Freq. Control **39**, 285–292 (1992).

[15]F. Reverdy and B. Audoin, "Elastic constants determination of anisotropic materials from phase velocities of acoustic waves generated and detected by lasers," J. Acoust. Soc. Am. **109**, 1965–1972 (2001).

[16]S. Enoch, G. Tayeb, P. Sabouroux, N. Guérin, and P. Vincent, "A metamaterial for directive emission," Phys. Rev. Lett. **89**, 213902 (2002).

[17]J. Zhang, Y. Luo, H. Chen, and B.-I. Wu, "Manipulating the directivity of antennas with metamaterial," Opt. Express **16**, 10962–10967 (2008).

[18]M.-H. Noroy, D. Royer, and M. Fink, "The laser-generated ultrasonic phased array: Analysis and experiments," J. Acoust. Soc. Am. **94**, 1934–1943 (1993).

[19]T. F. Crimmins, A. A. Maznev, and K. A. Nelson, "Transient grating measurements of picosecond acoustic pulses in metal films," Appl. Phys. Lett. **74**, 1344–1346 (1999).

[20]M. Kouyate, T. Pezeril, D. Mounier, and V. Gusev, "Generation of inhomogeneous plane shear acoustic modes by laser-induced thermoelastic gratings at the interface of transparent and opaque solids," J. Appl. Phys. **110**, 123526 (2011).

[21]H. Lamb, "On the propagation of tremors over the surface of an elastic solid," Philos. Trans. R. Soc. London, Ser. A **203**, 1–42 (1904).

[22]G. F. Miller and H. Pursey, "The field and radiation impedance of mechanical radiators on the free surface of a semi-infinite isotropic solid," Proc. R. Soc. London, Ser. A **223**, 521–541 (1954).

[23]A. E. J. Lord, "Geometric diffraction loss in longitudinal- and shear-wave attenuation measurements in an isotropic half-space," J. Acoust. Soc. Am. **39**, 650–662 (1966).

[24]J. D. Achenbach, *Reciprocity in Elastodynamics* (Cambridge University Press, Cambridge, 2003).

[25]Y. Guo, D. Yang, W. Feng, and Y. Chang, "Influence of transparent coating hardness on laser-generated ultrasonic waves," J. Appl. Phys. **113**, 023509 (2013).

[26]J. T. J. Cherry, "The azimuthal and polar radiation patterns obtained from a horizontal stress applied at the surface of an elastic half space," Bull. Seismol. Soc. Am. **52**, 27–36 (1962).

[27]I. N. Gupta, "Note on the use of reciprocity theorem for obtaining radiation patterns," Bull. Seismol. Soc. Am. **1965**, 277–281 (1965).

[28]I. N. Gupta, "Body wave radiation patterns from force applied within a half space," Bull. Seismol. Soc. Am. **56**, 173–183 (1966).

[29]S. T. Hocter, "Exact and approximate directivity patterns of the sound radiated from a cylindrical duct," J. Sound Vib. **227**, 397–407 (1999).

[30]C. R. Lowis, P. F. Joseph, and A. J. Kempton, "Estimation of the far-field directivity of broadband aeroengine fan noise using an in-

Redistribution subject to ASA license or copyright; see http://acousticalsociety.org/content/terms. Download to IP: 134.157.146.58 On: Fri, 10 Jan 2014 11:32:51

duct axial microphone array," J. Sound Vib. **329**, 3940–3957 (2010).
[31]D. A. Hutchins, R. J. Dewhurst, and S. B. Palmer, "Directivity patterns of laser generated ultrasound in aluminum," J. Acoust. Soc. Am. **70**, 1362–1369 (1981).
[32]J. R. Bernstein and J. B. Spicer, "Line source representation for laser-generated ultrasound in aluminum," J. Acoust. Soc. Am. **107**, 1352–1357 (2000).
[33]W. Yaping, S. Dufang, and H. Yulong, "Study of the directivity of laser generated ultrasound in solids," J. Appl. Phys. **83**, 1207–1212 (1998).
[34]B. Yuhai, P. Liwei, F. Qiping, Y. Yuping, and Y. Chongfu, "Experimental studies of directivity patterns of laser generated ultrasound in neutral glasses," Ultrasonics **33**, 429–436 (1995).
[35]S. Raetz, T. Dehoux, and B. Audoin, "Effect of laser beam incidence angle on the thermoelastic generation in semi-transparent materials," J. Acoust. Soc. Am. **130**, 3691–3697 (2011).
[36]C. B. Scruby and L. Drain, *Laser Ultrasonics: Techniques and Applications* (Adam Hilger, Bristol, 1990).
[37]V. E. Gusev and A. A. Karabutov, *Laser Optoacoustics* (AIP, New York, 1993).
[38]J. D. Achenbach, *Wave Propagation in Elastic Solids* (North-Holland Publishing Company, Amsterdam, 1973).
[39]Schott, "Schott datasheet on neutral density NG1 glass," technical report (2008).
[40]L. R. F. Rose, "Point-source representation for laser-generated ultrasound," J. Acoust. Soc. Am. **75**, 723–732 (1984).

Redistribution subject to ASA license or copyright; see http://acousticalsociety.org/content/terms. Download to IP: 134.157.146.58 On: Fri, 10 Jan 2014 11:32:51